Parity-symmetry breaking and topological phases in a superfluid ring

Xiurong Zhang,[1] Francesco Piazza,[2] WeiDong Li,[1,*] and Augusto Smerzi[3]
[1]*Institute of Theoretical Physics and Department of Physics, Shanxi University, 030006 Taiyuan, China*
[2]*Institut for Theoretische Physik, Universit Innsbruck, A-6020 Innsbruck, Austria*
[3]*QSTAR, INO-CNR and LENS, Largo Enrico Fermi 2, I-50125 Firenze, Italy*
(Received 5 August 2016; published 1 December 2016)

We study analytically the superfluid flow of a Bose-Einstein condensate in a ring geometry in the presence of a rotating barrier. We show that a phase transition breaking a parity symmetry among two topological phases occurs at a critical value of the height of the barrier. Furthermore, a discontinuous (accompanied by hysteresis) phase transition is observed in the ordered phase when changing the angular velocity of the barrier. At the critical point where the hysteresis area vanishes, the chemical potential of the ground state develops a cusp (a discontinuity in the first derivative). Along this path, the jump between the two corresponding states having a different winding number shows analogies with a topological phase transition. We finally study the current-phase relation of the system and compare some of our calculations with published experimental results.

DOI: 10.1103/PhysRevA.94.063601

I. INTRODUCTION

A paradigmatic manifestation of superfluidity is the existence of stationary atomic states in a ring geometry in the presence of a barrier rotating with constant angular velocity Ω [1]. With Bose-Einstein condensates (BECs), these states have been recently observed experimentally [2–6] and extensively studied theoretically [7–18]. The stationary current-carrying states are characterized by a topological invariant given by the phase of the superfluid accumulated around the ring $\nu = 2\pi\ell$, with the integer winding number $\ell = 0, \pm 1, \pm 2 \ldots$ [19]. The winding number can be dynamically modified by sweeping the angular velocity of the rotating barrier [5,6]. The change in topology takes place via the creation of topological defects (solitons in one dimension $d = 1$ [20] and vortices in $d > 1$ [10,14–16]).

In the limit of a vanishing barrier, the state with topological defects adiabatically connects two rotation-invariant states with different winding numbers ℓ. A second-order phase transition takes place two times as a function of Ω [20], first as the system enters the state with topological defects from the first rotational-invariant state ℓ_1 and then as it leaves the former by entering the second rotational-invariant state ℓ_2. This scenario changes in the presence of any finite-size obstacle that breaks the rotational symmetry of the ring, wherein the topological defects are always dynamically unstable [21], so that, in general, two topologically different states cannot be adiabatically connected. This has been recently confirmed experimentally with a barrier moving inside a toroidal BEC [22], where hysteresis appears in the transition between states with different topological winding numbers. The unstable branch of the hysteresis loop corresponds to the state with topological defects, and the angular velocity at which the metastable state decays (through phase slippage [7]) into the ground state generalizes the Landau critical velocity to the weak-link case [16,21].

In this paper, we show that with a barrier rotating at the angular velocity $\Omega_c = \hbar/2mR^2$, with R and m as the radius of the ring and the atomic mass, respectively, the ground state of the system becomes degenerate when the height of the barrier is smaller than a critical value $V < V_c$. The degeneration arises from a parity-symmetry breaking that provides two possible ground states with different topology, i.e., winding number. In the disordered phase, $V > V_c$, the ground state is unique with an undefined winding number. Furthermore, by keeping constant the height of the barrier in the ordered phase, $V < V_c$, a first-order phase transition between the two ground states with different topological winding number and hysteresis can be observed by varying Ω. The area enclosed by the hysteresis path shrinks while increasing the height of the barrier till eventually vanishing at the critical point $V = V_c$. Hysteresis has been experimentally observed but the sudden change in the winding number at Ω_c was smeared out due to shot-to-shot number and finite temperature fluctuations [22]. As order parameter of the phase, both the continuous and discontinuous phase transitions, we choose the difference between the phase accumulated around the ring ν and phase drop across the barrier, a quantity which is experimental accessible [23]. The phase drop across the barrier, together with the current flowing through the ring, also provides the current-phase relation [23,24]—an optimal characterization of the ring-superfluid junction [25–29].

We finally emphasize that at the angular velocity Ω_c and $V = V_c$ the transition between the two topological states is accompanied by a discontinuity in the derivative of the ground-state chemical potential as a function of the angular velocity. Furthermore, at this point the transition is not associated with the breaking of any symmetry and it cannot therefore be characterized by a local order parameter. This carries some similarities with a continuous topological phase transition occurring between two degenerate ground states with different topological winding numbers ℓ.

II. THE MODEL

We consider a BEC confined in an effective one-dimensional toroidal trap in the presence of a barrier rotating with a constant angular velocity Ω. The barrier is a penetrable repulsive potential with radial extension larger than the annulus

*Corresponding author: wdli@sxu.edu.cn

width. The system can be modeled by the Gross-Pitaevskii equation (GPE) [30] that governs the dynamics along the azimuthal coordinate $x \in [-L/2, L/2]$, where L is the length of the ring. We remove the time dependence of the Hamiltonian by moving to a rotating reference frame: $x \Rightarrow x + \Omega R t$ with the torus radius $R = L/2\pi$. This introduces a gauge field $\propto \Omega R$ into the GPE, which reads

$$i\hbar\frac{\partial}{\partial t}\Psi(x,t) = [\hat{H} + Ng|\Psi(x,t)|^2]\Psi(x,t),$$
$$\hat{H} = \frac{\hbar^2}{2m}\left(i\frac{\partial}{\partial x} + m\frac{\Omega R}{\hbar}\right)^2 + V(x) - \frac{1}{2}m\Omega^2R^2. \tag{1}$$

The barrier $V(x)$ is a repulsive square well with height $V > 0$ and width d centered about $x = 0$, N is the number of atoms, and $g = 4\pi\hbar^2 a_s/m$ is the contact interaction with the effective one-dimensional (1D) s-wave scattering length a_s. With the further transformation $\Psi(x,t) = e^{i(m\Omega Rx + m\Omega^2R^2t/2)/\hbar}\phi(x,t)$, the gauge field can be removed from the Hamiltonian which now reads as the usual nonlinear GPE for the order parameter $\phi(x,t)$ [31,32]. Following [24,28,33–37], the stationary solutions of Eq. (1) can be written in terms of one of Jacobi elliptical functions, SN function [38]. Two classes of solutions which we call, for reasons that will become clear below, plane waves (PWs) and solitons (SLs), are found for each value of the winding number ℓ. The circulation is $\nu = \oint \Theta(x)dx = 2\pi\ell$, where $\Theta(x) = m\Omega Rx/\hbar + \theta(x)$ is the phase in the laboratory frame while $\theta(x) = (m/\hbar)\int dx j/\rho(x)$ is the phase in the rotating frame. The BEC density is $\rho(x) = |\Psi(x)|^2 = |\phi(x)|^2$ and in the rotating frame the current j and the chemical potential ϵ are related with the current and chemical potential in the laboratory frame by $I(x) = j + \Omega R\rho(x)$ and $\mathcal{E} = \epsilon - m\Omega^2R^2/2$, respectively. In absence of the barrier, $V = 0$, the current for the PW solution is simply $I = \ell I_0$, where we choose $I_0 = R\Omega_0\rho_0$ and $\Omega_0 = \hbar/mR^2$ as units of the current and the rotation velocity and a density normalized as $\rho_0 = 1/L$. The SL state has a chemical potential larger than the chemical potential of the PW state $\mu_0 = Ng\rho_0$, which will be used to define our units of the energy, time $\hbar/\mu_0$, and length $\xi_0 = \hbar/\sqrt{2m\mu_0}$. The presence of a repulsive barrier breaks the rotational invariance, and the two solutions at fixed Ω, ν are not purely a PW or a SL. As already mentioned, we found two kinds of solutions that will be labeled as PW (SL) since both continuously reduce to an exact PW (SL) as $V \to 0$ [24].

III. CONTINUOUS PHASE TRANSITION

In the following we study the exact ground-state solutions as a function of the order parameter

$$\alpha = \nu - \gamma, \tag{2}$$

that is the difference between the circulation ν and the phase drop across the barrier γ [38]. In the limit $V = 0$, the phase difference is simply equal to the the phase accumulated around the ring: $\alpha = \nu = 2\pi\ell$. This quantity has been measured experimentally [23] from the interference fringes of two overlapping BECs, one expanding from a ring with a barrier and the second expanding from a disk without a barrier providing the reference phase.

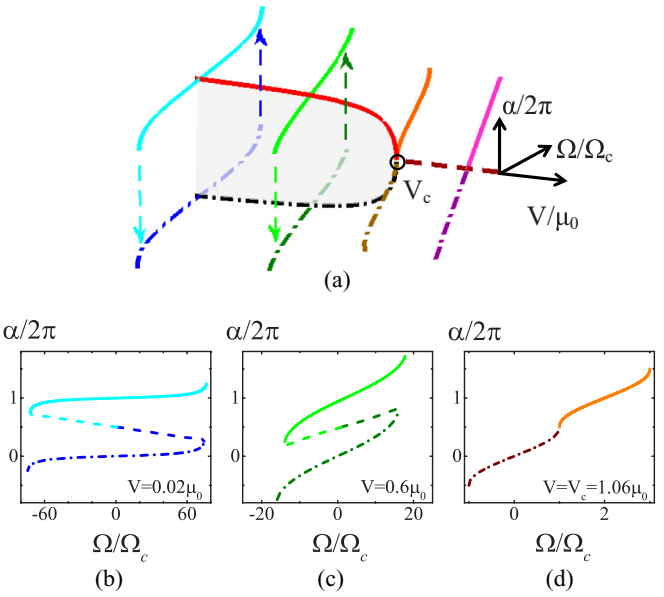

FIG. 1. Order parameter α as a function of the barrier angular velocity Ω and height of the barrier V. (a) At fixed $\Omega = \Omega_c$, the ground-state solution of the system becomes degenerate at $V < V_c$. The black dot-dashed line (the lower branch of the pitchfork bifurcation) and red solid line (the upper branch of the pitchfork bifurcation) correspond to the value of α for the PW branch with winding number $\ell = 0$ or 1, respectively, plotted as a function of V. At $V \geqslant V_c$, the order parameter vanishes and the winding number of the state is undefined, seeing the dashed line. Further solid or dot-dashed lines running along the Ω direction for different values of V give α also for the PW branch, where the different colors and line styles correspond to different winding number $\ell = 0$ (the dot-dashed lines) or 1 (the solid lines). Hysteresis along the closed trajectories marked by dark-light green (the right hysteresis loop) and dark-light blue (the left hysteresis loop) colors exists for $V < V_c$. (b–d) Value of α as a function of Ω for three different values of V. Solid and dot-dashed (dashed) lines correspond to the PW(SL) branch and different line styles correspond to different winding number $\ell = 0$ (the dot-dashed lines) or 1 (the solid lines). In (d), at $V = V_c = 1.06\mu_0$, the $\ell = 0$ and 1 PW branches are directly connected at a point where the derivative of α as a function of Ω diverges. Here the parameters are the same as in Fig. 3.

The phase diagram of the system is depicted in Fig. 1(a), where the order parameter α is plotted as a function of the angular velocity Ω and strength V. When $V < V_c$, the ground state is a PW with the winding number either $\ell = 0$ or 1 and is characterized by a nonvanishing α. This bifurcation is a pitchfork for $\Omega = \Omega_c$, with the unstable branch for $V < V_c$ being the SL solution [not shown in Fig. 1(a); see dashed lines in Figs. 1(b) and 1(c)]. For $\Omega \neq \Omega_c$ the bifurcation becomes a saddle node (see the discussion of Fig. 4 below). The behavior of α as a function of Ω is shown in Figs. 1(b)–1(d) for three different values of V, where the solid and dot-dashed (dashed) lines correspond to the PW (SL) branch and the different colors and line styles correspond to different winding numbers.

It is instructive to analyze how a nonvanishing order parameter α arises by looking at the particular spatial form of the solutions, shown in Fig. 2. For a fixed angular velocity Ω_c the behavior of the density and phase of the PW solution is

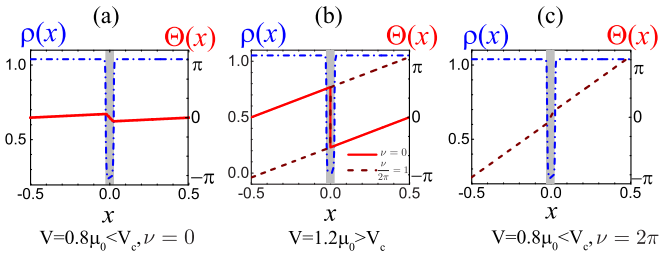

FIG. 2. Density and phase profiles of the PW solutions in the hysteretic regime (a) and (c) and in the nonhysteretic regime (b). The shaded area indicates the barrier region. Here the parameters are the same as in Fig. 3.

shown both inside and outside the hysteretic region. In absence of hysteresis, $V \geqslant V_c$, the $\nu = 0$ and 2π branches share the same density profile, characterized by a zero at the center of the weak link: $x = 0$. At this singular point, the phase has a π jump, downwards for the $\nu = 0$ branch, upwards for the $\nu = 2\pi$ branch, leading to the same value of α (see Fig. 1). For $x \neq 0$ the phase grows linearly with the same slope for both branches. The presence of a singular point (topological defect) in the PW branches indicates that the latter acquires a solitonic character in the nonhysteretic regime. The SL and PW branches for a given ν and Ω_c are indeed equal for $V \geqslant V_c$ and the winding number ℓ is not defined along this path [dashed line in Fig. 1(a)].

IV. DISCONTINUOUS PHASE TRANSITION AND HYSTERESIS

With a barrier height V below the critical value V_c the system supports hysteresis, as already experimentally demonstrated in [22]. In the region $\Omega < \Omega_{c1}$ the PW state with $\ell = 0$ has the lowest energy, while in the region $\Omega > \Omega_{c2}$ the lowest-energy state is a PW with $\ell = 1$. In the region $\Omega_{c1} < \Omega < \Omega_{c2}$ one of the PW solutions is stable while the other is metastable. The metastable PW branch is connected with the SL branch for $\Omega_{c1} \leqslant \Omega \leqslant \Omega_{c2}$, while outside this region only a single PW branch exists. The values of $\Omega_{c1,c2}$ are determined by the interaction strength gN and the height and the width of the barrier. The fact that the SL branch in this region is unstable explains the hysteretic behavior [16] (see the lower panel of Fig. 3): as soon as the PW branch meets the SL branch a dynamical instability sets in whereby the system decays into the lowest-energy PW branch having a different winding number. This dynamical instability originates from the underlying saddle-node bifurcation where the PW and the SL branch merge [21] (see also Fig. 4). We remark that in this case the change of the topological winding number ℓ, taking place while going from the metastable to the stable PW branch, is discontinuous.

The situation changes when $V \geqslant V_c$: in this case hysteresis is absent and the two PW branches with $\ell = 0$ and 1 are directly connected, without the intermediate unstable SL branch. Therefore, as shown in Fig. 3, at $\Omega = \Omega_c$ the topological winding number jumps between $\ell = 0$ and 1, while the system remains in the lowest-energy stationary state. Moreover, as evident from the upper panel of Fig. 3, if we additionally tune the barrier height to $V = V_c$ the chemical

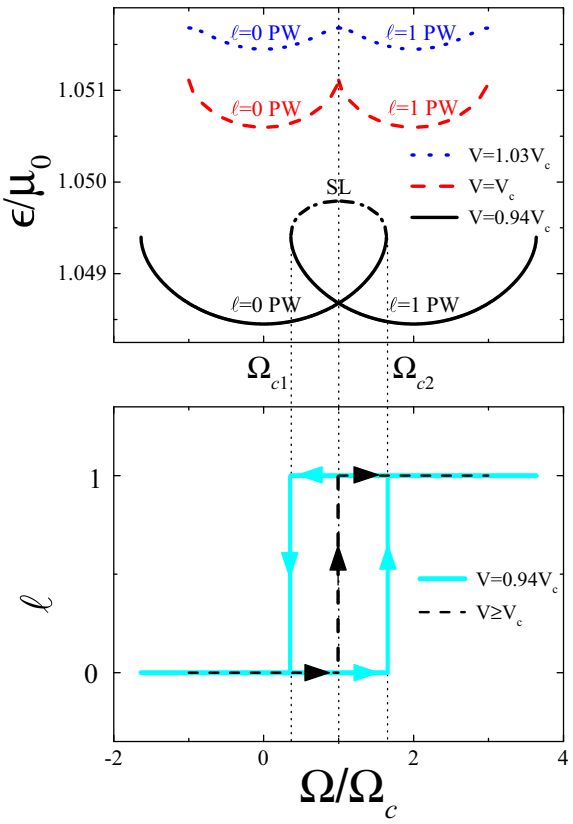

FIG. 3. Upper panel: chemical potential for three different values of the barrier height (in units of μ_0). Lower panel: topological winding number below and over the critical barrier height. Arrows highlight the hysteretic behavior as a function of the rotation velocity. Here $L = 20d$ and $d = 20\xi_0$, similarly to the NIST experiment [23].

potential shows a discontinuous derivative at $\Omega = \Omega_c$. This resembles a topological phase transition (a transition between two topologically distinct states) without breaking any local symmetry. This behavior is always present, independently of the particular form of the barrier.

The disappearance of hysteresis for high enough barriers has been observed experimentally [22]. Yet the observed transition between states with a different winding number was not perfectly sharp, probably due to shot-to-shot atom-number fluctuations. In order to verify our scenario involving a "topological" phase transition one would need to observe both (i) a sharp jump between $\ell = 0,1$ as a function of Ω and (ii) a second-order discontinuity in some observable (like the chemical potential shown in Fig. 3). In order to observe (i), the temperature has to be low enough to suppress random nucleation of topological defects [8]—as probably already being the case of [22]—and shot-to-shot number fluctuations need to be reduced. The measurement of a discontinuity in the derivative of the chemical potential as required in (ii) seems a more demanding task.

V. CURRENT-PHASE RELATION

The knowledge of the phase drop γ across the barrier, combined with the knowledge of the (spatially constant) current j flowing across the weak link, allows us to construct

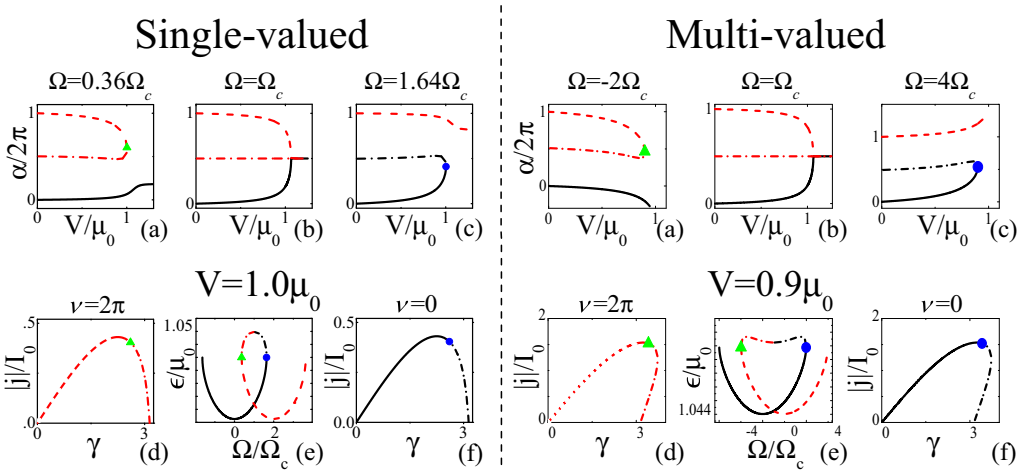

FIG. 4. Current-phase relation with a rotating barrier. Panels (a–c) show the order parameter α as a function of the barrier height V. Panels (d,f) show the current-phase relation, while panel (e) reports the chemical potential vs Ω. In (a,d,e) the black solid line represents the $\nu = 0$ PW branch, while the dashed and dash-dotted red line corresponds to the $\nu = 2\pi$ PW and SL branch, respectively. In (c,f), the red dashed line represents the $\nu = 2\pi$ PW branch while the solid and dash-dotted black line corresponds to the $\nu = 0$ PW and SL branch, respectively. In (b) the SL branches for $\nu = 0, 2\pi$ overlap. The blue circle and green triangles mark the special points (saddle-node bifurcations) where the PW and SL branch meet. In the left panel, the current-phase relation is single-valued, i.e., $\gamma < \pi$, while in the right panel it is multivalued, namely, for some values of the current j we have $\gamma > \pi$. Here the parameters are the same as in Fig. 3.

the current-phase relation of the system. This is a powerful characterization of the weak link, allowing us for instance to distinguish different regimes ranging from deep tunneling to hydrodynamic flow [25–27]. In the context of BECs, the current phase relation has been computed so far for infinite systems with open boundary conditions, a static weak link, and a given injected flow [24,39]. Stimulated by the experimental results in [23], we compute here the current-phase relation for our case of a BEC in a ring geometry. The results are shown in Fig. 4. For a given barrier, interaction strength, and winding number, the current-phase relation can be constructed by varying the angular velocity Ω. As illustrated above, for each fixed Ω, i.e., fixed current j, we obtain two solutions (PW and SL branches) with a different value of γ. The current-phase relation for both $\ell = 0$ and 1 is shown in Figs. 4(d) and 4(f) for two different values of the barrier height V. The current-phase relation is composed of the PW and SL branches, meeting at the special points indicated by blue circles or green triangles. The same points are marked also in the μ versus Ω diagram [panel (e)], as well as in the α versus V diagram [panels (a) and (c)]. It appears how those special points are saddle-node bifurcations, where the PW and SL branch merge and disappear so that there are no stationary solutions for larger (or smaller) values of V or Ω. In (b) we also show that at $\Omega = \Omega_c$ the bifurcation becomes a pitchfork, as previously discussed. The latter is characterized by the merging of four branches: the two PW branches with $\nu = 0, 2\pi$ (black solid and red dashed lines) and the two SL branches with $\nu = 0, 2\pi$ (red dash-dotted line), which have the same α.

The current-phase relation indicates the maximal current j and the largest phase drop γ for a given barrier. In the deep tunneling regime, the current-phase relation is sinusoidal, while in the hydrodynamic regime of flow, achieved for barriers much smaller than the chemical potential, the current is quite higher and linearly proportional to the phase drop over a broad range of phases [27]. Moreover, there is a further regime where the phase drop can be larger than π, which implies that the current-phase relation becomes multivalued, as shown in the right part of Fig. 4.

VI. COMPARISON WITH EXPERIMENTS

All the predictions presented in this paper can be experimentally tested within the experimental current state of the art. In this final section we compare some of our results with experimental results already obtained at NIST and published in [22,23]. The comparison is summarized in Fig. 5. Apart from the barrier width along the azimuthal coordinate, taken from [22,23], the most relevant parameter is the dimensionless effective nonlinearity:

$$\eta = N \times Lmg/\hbar^2.$$

As apparent from Figs. 5(a) and 5(b), the agreement between our predictions and the experimental data strongly depends on the value of η, determined by the total atom number N and ring length L. In (a) our predictions are calculated by taking $N = 8 \times 10^5$ and $L = 140\,\mu$m from [23] without any adjustable parameters, which clearly overestimates the size of the hysteresis loop. However, as shown in (b), a very good agreement could be provided, after reducing the effective nonlinearity η by 25%, as confirmed in (c) by comparing also the variation of α with the velocity Ω. Quite recently, it has been experimentally found a strong temperature dependence of the area of the hysteresis loops [40], in concomitance with an atom loss of about 20%. While the reduction of the condensate atoms can be qualitatively taken into account in our model, thermal fluctuations, that might also be crucially related with the area of the hysteresis loop, are well beyond the GPE approach investigated here. The fact that our purely 1D model overestimates the nonlinearity at given N, L also arises

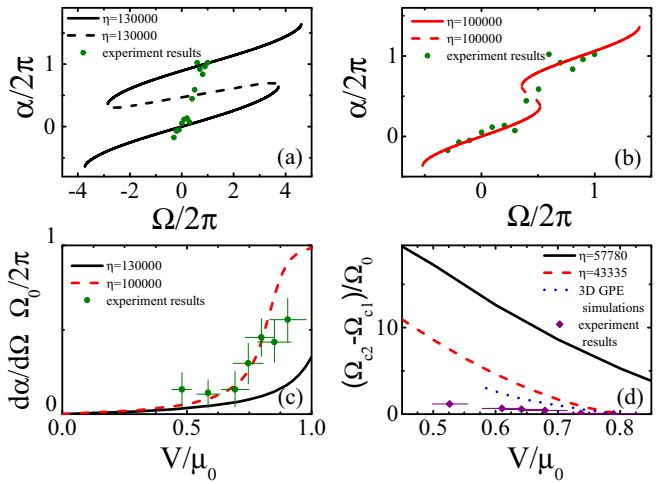

FIG. 5. Comparison with the experimental measurements of [23] for the order parameter α as a function of angular velocity Ω, (a) without and (b) with the fitted nonlinear parameter η (see text). (c) Rate of change of α as a function of barrier height V. In (d) the size of the hysteresis loop is compared to the value measured in [22] and to the full 3D GPE simulations (blue dotted line) employed in [22]; the black line corresponds to the predictions without fitting parameters, while the red lines correspond to the predictions with a nonlinearity η also reduced by 25%. In (a,b), the barrier height is $V = 0.8\mu_0$. In (a–c), the barrier width is chosen according to [23] to be $d \approx 0.04L \approx 22\xi_0$, while in (d) it is taken to be $d \approx 0.05L \approx 17\xi_0$, according to [22].

from the fact that the experiment is not in the one-dimensional regime. It is still possible to reproduce the experimental results even quantitatively by simply readjusting the effective nonlinearity, consistently with the comparison presented in [23], where an effective one-dimensional model showed a good agreement once the proper dimensional reduction was performed.

VII. CONCLUSIONS

We have studied the superfluid flow of a Bose-Einstein condensate confined in a ring geometry in presence of a rotating barrier. The stationary solutions have been found by solving analytically an effective one-dimensional Gross-Pitaevskii equation. We have identified a continuous parity-symmetry-breaking phase transition among two topological phases. A discontinuous phase transition accompanied by hysteresis as a function of the angular velocity of the barrier. Hysteresis has been experimentally observed at NIST [22,23]. At the critical point where the hysteresis area vanishes, the chemical potential of the ground state develops a cusp (a discontinuity in the first derivative). Along this path, the jump between the two corresponding winding numbers shows analogies with a topological phase transition. A good agreement between the order parameter α as a function of the angular velocity and the rate $d\alpha/d\Omega$ as a function of the height of the barrier and the area of the hysteresis has been found with published experimental data in [22,23] by readjusting the effective nonlinearity to take into account the fact that the experiment is not purely one dimensional.

ACKNOWLEDGMENTS

This work was supported by the National Natural Science Foundation of China (Grant No. 11374197), Program for Changjiang Scholars and Innovative Research Team in University of China (Grant No. IRT13076), and the Hundred Talent Program of Shanxi Province (2012).

[1] A. J. Leggett, Rev. Mod. Phys. **71**, S318 (1999).
[2] A. Ramanathan, K. C. Wright, S. R. Muniz, M. Zelan, W. T. Hill, C. J. Lobb, K. Helmerson, W. D. Phillips, and G. K. Campbell, Phys. Rev. Lett. **106**, 130401 (2011).
[3] S. Moulder, S. Beattie, R. P. Smith, N. Tammuz, and Z. Hadzibabic, Phys. Rev. A **86**, 013629 (2012).
[4] C. Ryu, P. W. Blackburn, A. A. Blinova, and M. G. Boshier, Phys. Rev. Lett. **111**, 205301 (2013).
[5] N. Murray, M. Krygier, M. Edwards, K. C. Wright, G. K. Campbell, and C. W. Clark, Phys. Rev. A **88**, 053615 (2013).
[6] K. C. Wright, R. B. Blakestad, C. J. Lobb, W. D. Phillips, and G. K. Campbell, Phys. Rev. Lett. **110**, 025302 (2013).
[7] F. Piazza, L. A. Collins, and A. Smerzi, Phys. Rev. A **80**, 021601(R) (2009).
[8] A. C. Mathey, C. W. Clark, and L. Mathey, Phys. Rev. A **90**, 023604 (2014).
[9] F. Piazza, L. A. Collins, and A. Smerzi, New J. Phys. **13**, 043008 (2011).
[10] F. Piazza, L. A. Collins, and A. Smerzi, J. Phys. B **46**, 095302 (2013).
[11] Marco Cominotti, Davide Rossini, Matteo Rizzi, Frank Hekking, and Anna Minguzzi, Phys. Rev. Lett. **113**, 025301 (2014).
[12] Davit Aghamalyan, Marco Cominotti, Matteo Rizzi, Davide Rossini, Frank Hekking, Anna Minguzzi, Leong-Chuan Kwek and Luigi Amico, New J. Phys. **17**, 045023 (2015).
[13] A. Roussou, G. D. Tsibidis, J. Smyrnakis, M. Magiropoulos, Nikolaos K. Efremidis, A. D. Jackson, and G. M. Kavoulakis, Phys. Rev. A **91**, 023613 (2015).
[14] A. I. Yakimenko, Y. M. Bidasyuk, M. Weyrauch, Y. I. Kuriatnikov, and S. I. Vilchinskii, Phys. Rev. A **91**, 033607 (2015).
[15] M. Kunimi and Y. Kato, Phys. Rev. A **91**, 053608 (2015).
[16] A. Munoz Mateo, A. Gallemi, M. Guilleumas, and R. Mayol, Phys. Rev. A **91**, 063625 (2015).
[17] M. Syafwan, P. Kevrekidis, A. Paris-Mandoki, I. Lesanovsky, P. Kruger, L. Hackermuller, and H. Susanto, arXiv:1512.07924.
[18] Y. Li, W. Pang, and B. A. Malomed, Phys. Rev. A **86**, 023832 (2012).
[19] A. J. Leggett, Rev. Mod. Phys. **73**, 307 (2001).
[20] R. Kanamoto, L. D. Carr, and M. Ueda, Phys. Rev. Lett. **100**, 060401 (2008).
[21] S. Finazzi, F. Piazza, M. Abad, A. Smerzi, and A. Recati, Phys. Rev. Lett. **114**, 245301 (2015).
[22] S. Eckel, Jeffrey G. Lee, Noel Murray, Charles W. Clark, Christopher J. Lobb, William D. Phillips, Mark Edwards, and G. K. Campbell, Nature (London) **506**, 200 (2014).

[23] S. Eckel, F. Jendrzejewski, A. Kumar, C. J. Lobb, and G. K. Campbell, Phys. Rev. X **4**, 031052 (2014).
[24] F. Piazza, L. A. Collins, and A. Smerzi, Phys. Rev. A **81**, 033613 (2010).
[25] A. Barone and G. Paterno, *Physics and Applications of the Josephson Effect* (Wiley, New York, 1982).
[26] K. K. Likharev, *Dynamics of Josephson Junctions and Circuits* (Gordon and Breach, New York, 1986).
[27] R. E. Packard, Rev. Mod. Phys. **70**, 641 (1998).
[28] A. Baratoff, J. A. Blackburn, and B. B. Schwartz, Phys. Rev. Lett. **25**, 1096 (1970).
[29] F. Sols and J. Ferrer, Phys. Rev. B **49**, 15913 (1994).
[30] L. P. Pitaevskii and S. Stringari, *Bose-Einstein Condensation* (Clarendon, Oxford, 2001).
[31] B. Bransden and C. Joachain, *Quantum Mechanics*, 2nd ed. (Pearson Education, Upper Saddle River, New Jersey, 2000), p. 255.
[32] L. D. Landau and E. M. Lifshitz, *Quantum Mechanics (Non-Relativistic Theory)*, 3rd ed. (Pergamon, New York, 1977), p. 52.
[33] Yu. G. Mamaladze and O. D. Cheishvili, Zh. Eksp. Teor. Fiz. **50**, 169 (1966) [Sov. Phys. JETP **23**, 112 (1966)].
[34] S. Langer and V. Ambegaokar, Phys. Rev. **164**, 498 (1967).
[35] B. T. Seaman, L. D. Carr, and M. J. Holland, Phys. Rev. A **71**, 033609 (2005).
[36] WeiDong Li, Phys. Rev. A **74**, 063612 (2006).
[37] W. D. Li and A. Smerzi, Phys. Rev. E **70**, 016605 (2004).
[38] See Supplemental Material at http://link.aps.org/supplemental/10.1103/PhysRevA.94.063601 for a discussion of the details of the analytical solutions of GPE (1) and the proof of Eq. (2).
[39] G. Watanabe, F. Dalfovo, F Piazza, L. P. Pitaevskii, and S. Stringari, Phys. Rev. A **80**, 053602 (2009).
[40] A. Kumar, S. Eckel, F. Jendrzejewski, and G. K. Campbell, arXiv:1608.02894.